Separation and Purification Technology 322 (2023) 124304

Contents lists available at ScienceDirect

Separation and Purification Technology

journal homepage: www.elsevier.com/locate/seppur

Efficient cavity-enhanced adsorption and recovery of low-concentration ammonia on pillar[5]arenes

Wen-Qiang Gong, Yu-Xuan Fu, Yan Zhou, Ming-Shuai Sun *, Zhang-Min Li, Nai-Hao Lu, Duan-Jian Tao *

National Engineering Research Center for Carbohydrate Synthesis, Key Laboratory of Fluorine and Silicon for Energy Materials and Chemistry of Ministry of Education, College of Chemistry and Chemical Engineering, Jiangxi Normal University, Nanchang 330022 China

ARTICLE INFO

Keywords:
Ammonia capture
NH_3
Pillar[5]arenes
Solid adsorbent

ABSTRACT

Ammonia (NH_3) capture has great implications for environmental protection and resource recovery. Developing effective and recyclable adsorbent materials to remove low-concentration NH_3 in industrial waste gas is critical. Here, solid adsorbents per-hydroxylated pillar[5]arene (OHP[5]) and pillar[5]quinone (P[5]Q) with well-designed functional groups were synthesized and evaluated for NH_3 adsorption. The results showed that both materials have high NH_3 uptake capacity and excellent cycle stability. P[5]Q showed higher NH_3 capacity (15.4 mmol/g) than OHP[5] (11.5 mmol/g) at ambient conditions (293.2 K and 1.0 bar). Dynamic breakthrough experiments showed that P[5]Q had good separation performance on low concentration NH_3. Characterizations (including FTIR, SEM, and XPS) and density functional theory (DFT) studies revealed that the adsorption strength for NH_3 on P[5]Q possessing C═O groups was stronger than OHP[5] composed of phenolic hydroxyls. Also, the electron-accepting C═O groups on P[5]Q could change the intramolecular charge distribution, in which an amount of NH_3 enters and stores in the electron-deficient internal cavity of P[5]Q. It is demonstrated that P[5]Q with the suitable cavity has good potential for separating low concentration NH_3 from industrial waste gas.

1. Introduction

NH_3 is an important industrial raw material for fertilizers, explosives, and many other chemical commodities [1,2]. Due to its high hydrogen content and easy liquefaction for transportation, NH_3 is also used as an attractive renewable energy carrier [3–5]. On account of the wide application, more than 10 million tons NH_3 is released into the atmosphere every year as industrial waste. The concentration of NH_3 in those waste gas often ranges from 450 ppm to 30,000 ppm [6,7]. As a result, a huge amount of low-concentration NH_3 was discharged into the atmosphere, leading to serious environmental pollution [8–12]. For example, the release of NH_3 into the atmosphere will cause PM 2.5, eutrophication of water and other problems, causing serious damage to the environment. Therefore, the capture and recovery of low-concentration NH_3 are critical to environmental protection and the economy.

Absorbent has been widely used in capturing NH_3 from industrial emissions. Therefore, the design and preparation of absorbents are critical to the effective capture and recovery of NH_3. Liquid absorbent has the advantage of continuous operation and is widely used in industry. The most commonly used liquid absorbents are ionic liquids (ILs) and deep eutectic solvents (DESs). ILs are room-temperature molten salts widely used in the gas separation process with the advantages of low vapor pressure, well solubility, and designable structures [13–15]. For example, Zhang et al. designed a class of functionalized ionic liquids by introducing multiple protic hydrogen on triazole. The ionic liquid has the highest NH_3 absorption capacity among current absorbers, and its NH_3 absorption capacity can reach 0.365 g/g at 303.2 K and 1.0 bar [16]. However, ILs also exhibit some serious shortcomings that cannot be ignored, such as high viscosity after absorption, high costs, and difficult desorption, limiting their industrial application. DESs, with abundant hydrogen bond donors and acceptors, have been applied to the absorption and separation of NH_3 gas [17–19]. It is easier to prepare and costs less than ILs. However, the absorption of low concentration of NH_3 by DES is not entirely satisfied because of the lower capture efficiency.

Compared with liquid absorbents, solid phase adsorbents are more widely used in the selective separation of gases because of their large specific surface area, tunable porosity, and especially better stability.

* Corresponding authors.
E-mail addresses: mingshuaisun@jxnu.edu.cn (M.-S. Sun), djtao@jxnu.edu.cn (D.-J. Tao).

https://doi.org/10.1016/j.seppur.2023.124304
Received 23 April 2023; Received in revised form 29 May 2023; Accepted 6 June 2023
Available online 10 June 2023

Current reported solid materials include active carbon, zeolites, metal–organic frameworks (MOFs), covalent organic frameworks (COFs), hydrogen-bonded organic frameworks, etc [20–24]. Recently, Liu and his co-workers reported a class of zirconium-based MOF materials with a capacity of 10.6 mmol/g for NH_3 capture at 298 K and 1.0 bar [25]. Barin et al. demonstrated that strongly acidic chemisorption sites have good capture performance for the adsorption of NH_3 in ppm-level, and the prepared Brønsted acidic porous polymers with a remarkable adsorption capacity of up to 18.7 mmol/g for NH_3 at 298 K and 1.0 bar [26]. Li et al. prepared a class of ionic hybrid materials by impregnating ionic liquid into MOFs. Through the coordination between metal sites and NH_3 and hydrogen bonding, the adsorption capacity of NH_3 can reach 9.9 mmol/g at 353.2 K and 0.1 bar [27]. Kim et al. developed a class of MOF materials with open metal sites for NH_3 adsorption, which had extremely excellent adsorption capacity. The adsorption capacity of Mg_2(dobpdc) on NH_3 reached 23.9 mmol/g at 298.2 K and 1.0 bar, and 8.25 mmol/g at 570 ppm [28]. However, the strong binding of NH_3 to the acidic sites makes it difficult to desorb. Hence, high temperatures are usually required. The strong interaction also leads to irreversible damage to the cycle stability of the material.

Pillar[n]arenes, a new class of solid phase adsorbents, have attracted the attention of many gas separation researchers since their first discovery in 2008 by Ogoshi et al [29]. These special materials have columnar structures and fixed-size electron-rich cavities. Pillar[n]arenes have shown excellent and promising performance in the field of gas separation. Zhou et al. demonstrated the excellent performance of different functionalized pillar[5]arenes in the organic molecular separation [30–33]. Tan et al. showed that pillar[5]arene-based supramolecular organic frameworks enable storage and selective separation of high hydrocarbons [34]. The adsorption capacities for C_2H_2, C_2H_4, and CH_4 were 36, 23, and 16 cm^3/g, respectively. The adsorption selectivity of C_2H_2/H_2 mixed gas exceeds 10,000 at 273 K and 1.0 bar. Huang et al. reported that a class of pillar[n]arene (n = 5–6) can selectively remove trace isomers in chlorobutane through crystal transformation [35]. Therefore, compared with porous adsorbents, the unique fixed-size cavity of pillar[n]arenes can facilitate the mass transfer in the adsorption process and result in a relatively high adsorption selectivity, which makes pillar[n]arenes as promising candidates in low concentration NH_3 capture.

Herein, per-hydroxylated pillar[5]arene (OHP[5]) with five hydroquinone rings and its oxidized form pillar[5]quinone (P[5]Q) were prepared to test their performance with regard to low-concentration NH_3 adsorption. The prepared pillar[5]arenes both showed satisfactory adsorption performance for low-concentration NH_3, and the oxidation made P[5]Q better than OHP[5] in adsorbing NH_3. DFT analysis was also conducted to reveal the mechanism of the better performance of P[5]Q.

2. Experimental section

2.1. Materials

1,4-Dimethoxybenzene (99 %), paraformaldehyde (95 %), boron trifluoride diethyl etherate (98 %) ($BF_3O(C_2H_5)_2$), and boron tribromide (BBr_3) (99 %) were purchased from Shanghai Macklin Biochemical Co., Ltd. 1,2-Dichloroethane (AR) and chloroform (AR) were purchased from Tianjin Zhiyuan Chemical Reagent Co., Ltd·NH_3 (99.99 %), N_2 (99.99 %) and He (99.99 %) were purchased from Jiangxi Huahong Special Gas Co., Ltd. 1,2-Dichloroethane and chloroform were treated with 4A molecular sieve for water removal. Other chemicals were used as purchased without further treatment.

2.2. Adsorbent preparation

The precursor dimethoxypillar[5]arene (DMP[5]) was prepared following the procedure in the literature [36], then from there, OHP[5] and P[5]Q were synthesized sequentially as shown in Scheme 1. For the synthesis of DMP[5], paraformaldehyde (0.93 g) and 1,4-dimethoxybenzene (1.38 g) were added into the solvent 1,2-dichloroethane (20 mL). Then, 1.25 mL of $BF_3O(C_2H_5)_2$ was added dropwise to the above solution. The mixture was stirred for 0.5 h at room temperature and quenched with distilled water. Finally, the obtained DMP[5] product was isolated by column chromatography (solvent: petroleum ether/CH_2Cl_2 = 1:3, yield: 60 %).

For the synthesis of OHP[5], 2.51 g of BBr_3 and 0.25 g of DMP[5] were added into 30 mL chloroform, followed by stirring for 72 h at room temperature. After that, water was poured into the solution to produce the white precipitate. The white precipitate was rinsed with chloroform and hydrochloric acid (0.5 mol/L) to remove impurities and dried under vacuum for 12 h to obtain the pure OHP[5] powder. It is well known in organic chemistry that phenols are easily oxidized to benzoquinones. As shown in Figure S1, after being exposed to air for 24 h, white OHP[5] power was gradually oxidized to reddish-brown power P[5]Q. This color change is a characteristic color change during the oxidation of phenolic hydroxyl groups to benzoquinones [37]. As a result, the yield of P[5]Q was 54 % and it was dried at 353.2 K before use.

2.3. Characterizations

The ^1H and ^{13}C NMR spectra of pillar[5]arenes were recorded on a Bruker Avance III spectrometer at 400 MHz. Fourier transform infrared (FTIR) spectra were obtained on a Nicolet 6700 spectrometer. The thermogravimetric analysis (TGA) of pillar[5]arenes was tested on PerkinElmer Diamond TG/DTA apparatus under a nitrogen (N_2) atmosphere. The morphological features of pillar[5]arenes were examined by scanning electron microscope (SEM) on S-3400 electron microscope and transmission electron microscopy (TEM) on JEOL JEM-2100 electron microscope, respectively. The surface areas of pillar[5]arenes were recorded by N_2 adsorption/desorption analysis at 77 K on a Micromeritics Tristar II 3020 Instrument. The surface elemental composition of pillar[5]arenes was examined on AXIS Supra X-ray photoelectron spectroscopy (XPS, Kratos Analytical).

2.4. Gas adsorption experiments

The adsorption experiments of NH_3 on pillar[5]arenes were carried out on a self-made adsorption apparatus, as illustrated in Figure S2. The detailed procedure followed our previous work [38]. For desorption, pillar[5]arenes saturated with NH_3 were first placed at 363.2 K and 0.05 bar for 2 h in a stainless vacuum tank, then cooled down to room temperature for the following experimental tests. The breakthrough experiment of pillar[5]arenes for NH_3 adsorption was measured on a self-made breakthrough apparatus at 303.2 K as shown in Figure S3. The pillar[5]arenes sample (0.3 g) was put in the furnace tube, and the system temperature was kept at 353.2 K for 0.5 h under argon atmosphere to remove the possible water adsorbed on the pillar[5]arenes sample. Then, the mixed gas composed of 0.3 % NH_3 and 99.7 % N_2 was passed at a flow rate of 30 mL min^{-1} for the adsorption of NH_3 at 298.2 K and 1.0 bar. The gas flows were controlled at the inlet by a mass flow meter, and the composition of outlet gas was measured by the gas chromatograph-mass spectrometry (GCMS − QP2010 SE).

2.5. Computational details

DFT calculations were conducted to investigate the adsorption mechanisms of OHP[5] and P[5]Q with NH_3 using the Gaussian 16 software package [39]. Structures were optimized, and relevant energies were computed. All simulations were performed using the M06-2X functional combined with 3-zeta basis sets. Geometry optimization was carried out with an SDD basis set. The energy of the optimized structure was performed in a separate single-point calculation with M06-2X/def2-TZVP level of theory for better accuracy [40–42]. The

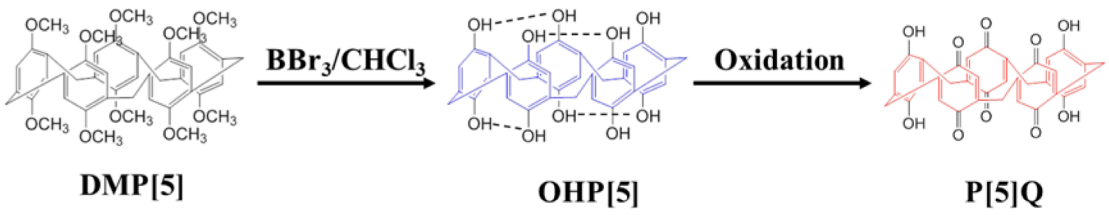

Scheme 1. The synthesis process of pillar[5]arenes.

binding energy (ΔE_b) of NH_3 and pillar arene was corrected by the basis set superposition error (BSSE) of OHP[5] or P[5]Q interacting with NH_3, which is defined as follows: $\Delta E_b = E_{PN} - E_P - nE_N + \Delta E_{BSSE}$. Where in the equation of ΔE_b, two fragments *P* and *N* were separately indicating OHP [5] (or P[5]Q) and NH_3. Isosurface maps of electrostatic potential (ESP) were displayed using the Visual Molecular Dynamics (VMD) visualization program based on the files exported by Multiwfn 3.8(dev) code [43].

3. Results and discussion

3.1. Characterization

The FTIR spectra of OHP[5] and P[5]Q are shown in Fig. 1. In general, the spectra patterns of the two samples are very similar. The characteristic of OHP[5] and P[5]Q were found around the intensity of peaks at 1435 cm^{-1}, 1196 cm^{-1}, and 932 cm^{-1}, which are attributed to C—OH bending, [44,45] C—O stretching vibration,[46] and C—H out-of-plane vibration, [47] respectively. The weaker intensities of the three peaks in P[5]Q are most likely due to the oxidation of the phenolic hydroxyl groups on OHP[5], affecting the vibration of corresponding structures. Besides the differences in intensities, OHP[5] shows a peak at 1340 cm^{-1}, corresponding to the vibration of O—H,[48] but not in the spectrum of the more oxidized P[5]Q. In contrast, a new peak at 1648 cm^{-1} is observed for P[5]Q, which can be ascribed to the in-plane stretching vibration of the quinone carbonyl group (C═O) [49,50]. Moreover, Figures S4-S9 show the ^1H and ^{13}C NMR spectra of DMP[5], OHP[5], and P[5]Q. It is found that the phenolic hydroxyl group on OHP [5] was oxidized into a quinoid structure on P[5]Q, confirming the successful oxidation treatment of OHP[5] to form P[5]Q. SEM images were presented in Fig. 2 to illustrate the morphology of DMP[5], OHP [5], and P[5]Q. DMP[5] showed an irregular morphology (Fig. 2a).

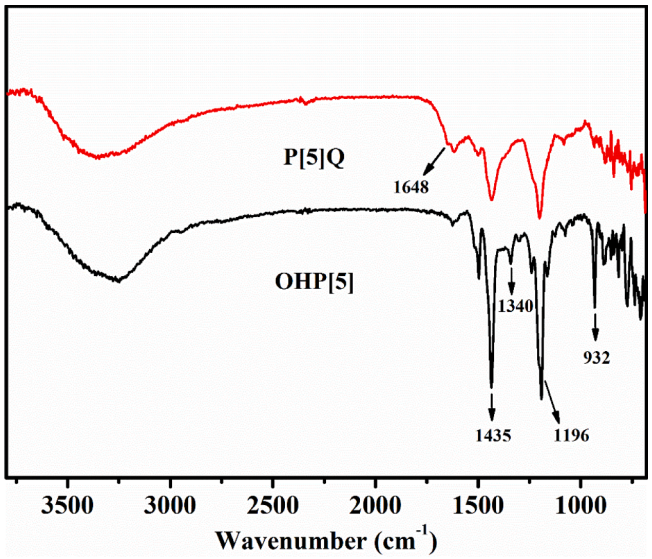

Fig. 1. FTIR spectra of OHP[5] and P[5]Q.

After the demethylation of DMP[5], the obtained OHP[5] demonstrated a rod-like structure (Fig. 2b). The rod-like structure was retained after oxidation treatment of OHP[5] to form P[5]Q (Fig. 2c). TEM results (Figure S10) also support the lack of hollow structures in the three pillar [5]arenes materials.

N_2 adsorption–desorption analysis was carried out to further understand the pore distribution of pillar[5]arenes (Fig. 3). It is demonstrated that the three pillar[5]arenes show similar type IV isotherm with the hysteresis loop H4 [51]. The results show that there are stacked slit pores in the three pillar[5]arenes. The adsorbed N_2 is slightly different among the three species, with the most for P[5]Q and the least for DMP [5] due to their specific surface area (DMP[5]: 21 m^2/g, OHP[5]: 27 m^2/g, and P[5]Q: 40 m^2/g). Their similarly low specific surface areas indicate that demethylation and oxidation processes have an insignificant effect on the surface areas of these three pillar[5] arenes. The thermal stability of the three pillar[5] arenes was further investigated by TGA. As shown in Figure S11, the three pillar[5]arenes were found to be highly stable under 450 K, demonstrating good thermal stability.

3.2. NH_3 adsorption performance

As one of the important indexes to evaluate the performance of adsorbents, it is necessary to test the adsorption rate. The adsorption rate curves of NH_3 on the three pillar[5]arenes were determined at 293.2 K and 1.0 bar, as shown in Fig. 4. The adsorption equilibrium was reached quickly, with approximately 3 min. The low surface area and lack of abundant pores can decrease gas diffusion resistance, which may explain the quick adsorption of NH_3 to reach equilibrium. After reaching the adsorption equilibrium, the sequence of NH_3 adsorption capacity is P[5]Q > OHP[5] > DMP[5]. The highest adsorption capacity of P[5]Q for NH_3 can reach 15.4 mmol/g, and that of OHP[5] and DMP[5] for NH_3 is 11.5 mmol/g and 4.1 mmol/g, respectively. That is to say, OHP[5] obtained by demethylation of DMP[5] owns many phenolic hydroxyl, which can facilitate to capture more NH_3 molecules. Notably, P[5]Q obtained by oxidation of OHP[5] have lots of C═O groups, which leads to the highest NH_3 adsorption capacity. The absence of phenolic hydroxyl and C═O groups in the molecular structure of DMP[5] is the main reason of its lowest performance. The oxidation of OHP[5] to P[5]Q (phenolic hydroxyls oxidized to benzoquinones) can further improve the adsorption performance of P[5]Q for NH_3 capture.

The influence of temperature and pressure on adsorption capacity of adsorbents were further researched. Fig. 5 shows the NH_3 adsorption performance of DMP[5], OHP[5], and P[5]Q under varying temperature or pressure conditions. When the pressure increases from 1 to 10 kPa, NH_3 adsorption performance of DMP[5] has little change (0.82–1.80 mmol/g), but the adsorption performance of NH_3 by OHP[5] (2.68–6.43 mmol/g) and P[5]Q (2.86–7.51 mmol/g) increases significantly (Fig. 5a). And the temperature effect on the adsorption capacity of NH_3 on P[5]Q was also examined and displayed in Fig. 5b. It is found that NH_3 adsorption capacity decreases with increasing temperature, which means the adsorption process of NH_3 is exothermic. In addition, considering that there are usually some other competing gases such as N_2 and CO_2 in the tail gas, the adsorption capacities of competitive gases N_2 and CO_2 on OHP[5] and P[5]Q were also examined at 293.2 K. The results were shown in Figure S12 and Figure S13. The adsorption

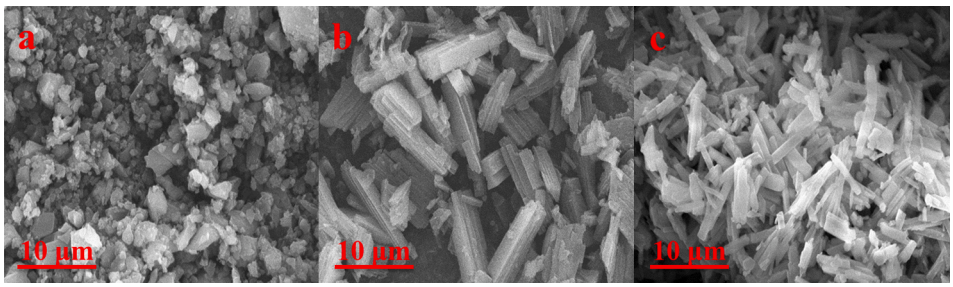

Fig. 2. SEM images of DMP[5] (a), OHP[5] (b), and P[5]Q (c).

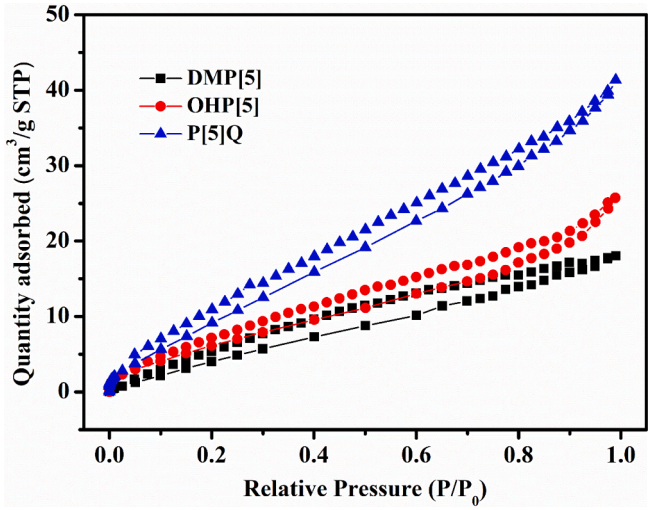

Fig. 3. N_2 adsorption–desorption isotherms of DMP[5], OHP[5] and P[5]Q.

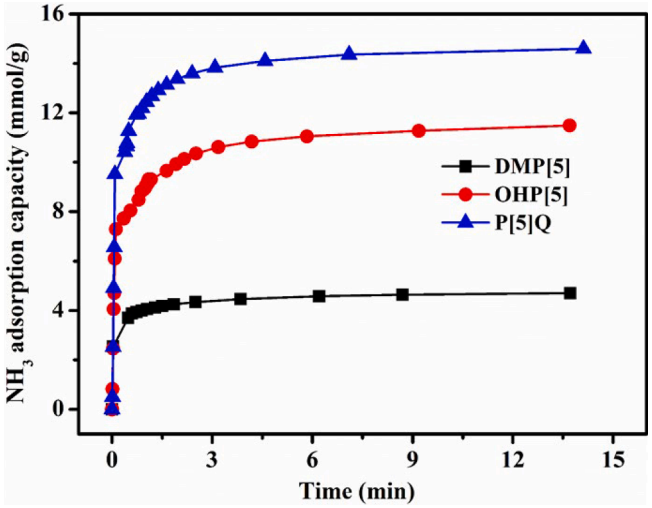

Fig. 4. Adsorption rates of NH_3 on DMP[5], OHP[5], and P[5]Q at 293.2 K and 1.0 bar.

capacity of OHP[5] for NH_3 was as high as 11.5 mmol/g at 293.2 K and 1.0 bar, which was only 0.106 mmol/g and 0.17 mmol/g for N_2 and CO_2 respectively. Similar to OHP[5], P[5]Q also had a very low capacity in the adsorption of pure N_2 (0.013 mmol/g) or CO_2 (0.196 mmol/g) in comparison with NH_3 adsorption (15.4 mmol/g), implying their good potential for selective adsorption of NH_3 from those two competitive gases.

3.3. Dynamic breakthrough performance

To evaluate the low concentration NH_3 separation performance of pillar[5]arene with industrial gases, experiments with similar gas compositions, 0.3 % NH_3/99.7 % N_2 gas mixture was used as feed gas (30 mL/min), were conducted at 303.2 K and 1.0 bar. The results (Fig. 6) show that P[5]Q can perfectly separate the two gases with NH_3 adsorbed on the solid and N_2 released. It suggests no degradation of material separation performance due to the competitive adsorption of N_2 during the separation process. The breakthrough time of NH_3 is as long as 120 min/g. This further confirms that P[5]Q has good performance for NH_3 separation at low concentration.

3.4. Adsorption mechanism

In order to further explain the mechanism of adsorption of NH_3 by pillar[5]arenes, the interaction between NH_3 and P[5]Q was investigated by XPS (Fig. 7). It is observed from Fig. 7a that a characteristic XPS peak signal of the N element appeared on the full spectrum after NH_3 adsorbed on P[5]Q, which indicates that P[5]Q interacts with NH_3. Moreover, Fig. 7b shows the deconvoluted C 1s spectra. Before NH_3 adsorption, P[5]Q shows two peaks in the C 1s region at 286.07 eV and 288.05 eV corresponding to C—O and C═O, respectively [52–54]. They shift to 285.96 eV (0.11 eV lower, C—O) and 288.23 eV (0.18 eV higher, C═O) after NH_3 adsorption (Fig. 7a). This indicates the existence of C—O—H···NH_3 interaction, which increases the electron density of the C atom. Similarly, the presence of C═O···H-NH_2 interaction reduces the electron density of the C atom. These findings show that phenolic hydroxyls and C═O groups are the key adsorption sites on P[5]Q for NH_3 capture. Moreover, the FTIR spectra characterization for P[5]Q before and after NH_3 capture was also carried out. As shown in Figure S14, the peak at 1648 cm^{-1} for fresh P[5]Q was observed, which is attributed to the stretching vibration of the quinone carbonyl group (C═O). After capture of NH_3, the vibration frequency of the quinone carbonyl group (C═O) was obviously red-shifted to 1640 cm^{-1}, confirming the NH_3···O═C interaction between the quinone carbonyl group and NH_3 molecule.

Experimental results have shown that the NH_3 adsorption capacity on P[5]Q is significantly higher than that on OHP[5], likely due to the stronger adsorption of NH_3 by quinone groups than by phenolic hydroxyls. To gain a better understanding at the molecular level, DFT calculations were performed to study the structure and energetic properties. The adsorption energy of NH_3 on P[5]Q is computed to be −24.2 kJ/mol, which is 0.5 kJ/mol lower than that on OHP[5] (–23.7 kJ/mol), indicating a more stable adsorption structure on P[5]Q. This suggests that P[5]Q holding benzoquinones structure can result in binding of more NH_3 molecules. Moreover, Fig. 8 shows ESP analysis on the van der Waals surface (0.001 a.u. contours of electronic density) of the optimized structures of OHP[5] and P[5]Q before and after loaded NH_3. It is worth noting that the ESP plots show an opposite charge for the internal channel of OHP[5] and P[5]Q. The internal channel of OHP[5] surrounded by benzene rings is negatively charged (Fig. 8a, color in blue), while the molecular channel inner wall of P[5]Q is positively charged

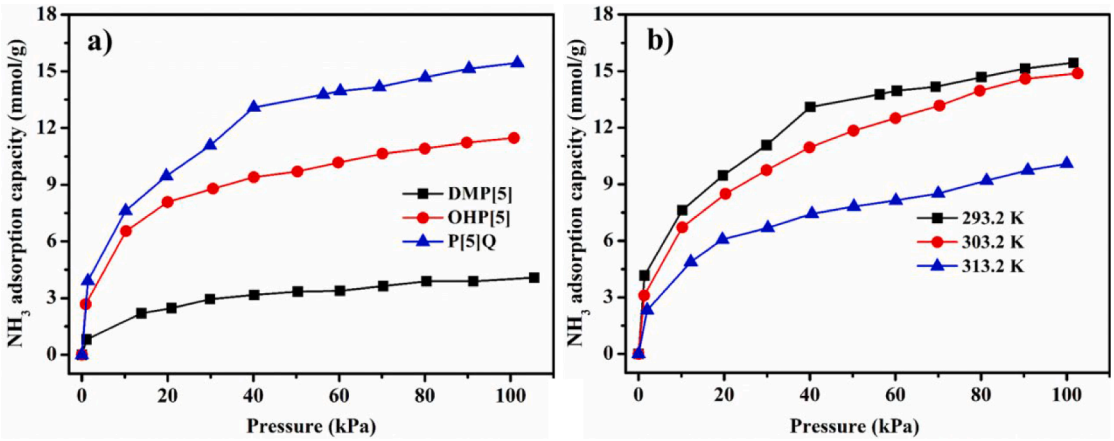

Fig. 5. (a) The adsorption capacity of NH_3 on the three pillar[5] arenes at 293.2 K, and (b) the adsorption capacity of NH_3 on P[5]Q at different temperatures.

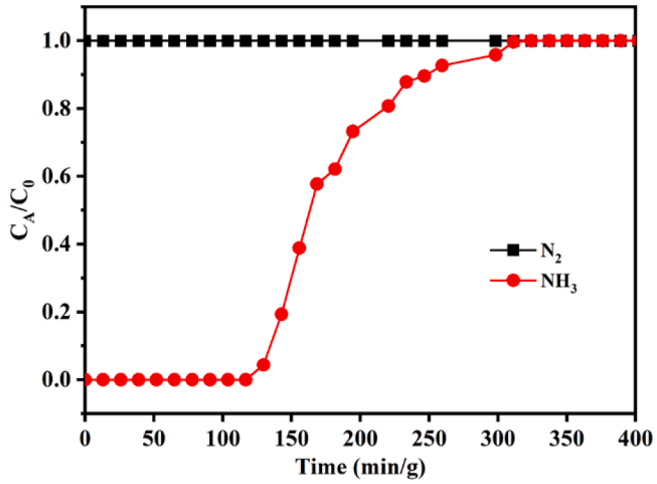

Fig. 6. NH_3 breakthrough curves on P[5]Q at 303.2 K and 1.0 bar.

(Fig. 8c, color in red). This finding demonstrates that the transformation of hydroxyl group on OHP[5] to quinone carbonyl group on P[5]Q causes the charge transfer in the cavity. The electron-accepting C═O groups on P[5]Q can attract the π electron from the benzene ring and change the intramolecular charge distribution, resulting the electron-deficient internal cavity of P[5]Q. Besides, the internal cavity diameter (0.56 nm) of P[5]Q is larger than the kinetic diameter (0.3 nm) of NH_3 molecules. As a result, the feature of electron-deficient internal cavity with a suitable diameter induces NH_3 molecules to enter the internal cavity of P[5]Q with an amount of NH_3 storage (Fig. 8d). However, NH_3 will be repelled inside the internal cavity of OHP[5] and can only stay at the edge of the molecular channel of OHP[5] as illustrated in Fig. 8b. This might be the microscopic reason for the higher NH_3 adsorption capacity on P[5]Q than on OHP[5].

3.5. Cycle performance

Recycling stability is of great importance for potential applications of adsorbent. Ten cycles of NH_3 adsorption–desorption by P[5]Q were performed to investigate the reusability of P[5]Q. The NH_3 desorption temperature was set as at 363.2 K. As shown in Fig. 9, P[5]Q kept as high as 92 % of the initial NH_3 uptake capacity after ten cycles. Moreover, the capacity of NH_3 adsorption becomes nearly constant during 2–10 runs. The FT-IR spectra of reused P[5]Q was supplemented in Figure S15. As shown in the figure, the FT-IR spectra of P[5]Q did not change significantly after regeneration. This indicates the excellent stability of P[5]Q in the application of NH_3 capture and recovery. This indicates the excellent stability of P[5]Q in the application of NH_3 capture and recovery. However, many reported adsorbents usually show poor cycle NH_3 adsorption performance. For example, MFM-303(Al) had a 40 % loss of the initial NH_3 adsorption amount after one cycle [55]. Otherwise, overhigh desorption temperature (e.g., 473.2 K) must be required for completely releasing adsorbed NH_3 [56]. Such higher temperature would easily lead to a serious structural collapse. Therefore, fast adsorption rate, high adsorption selectivity, mild desorption conditions and good cycle performance would make P[5]Q more attractive in NH_3 capture and recovery.

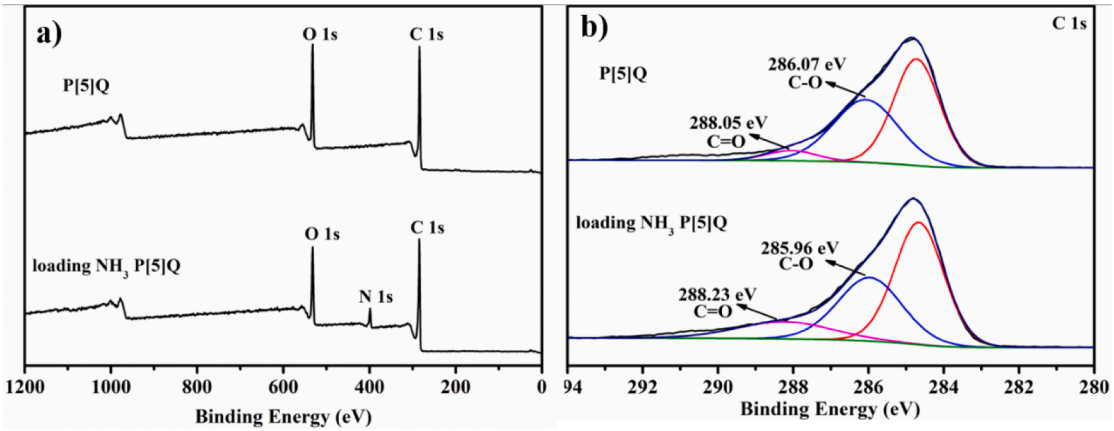

Fig. 7. (a) Full elemental XPS spectra and (b) C 1s of fresh P[5]Q and P[5]Q with adsorbed NH_3.

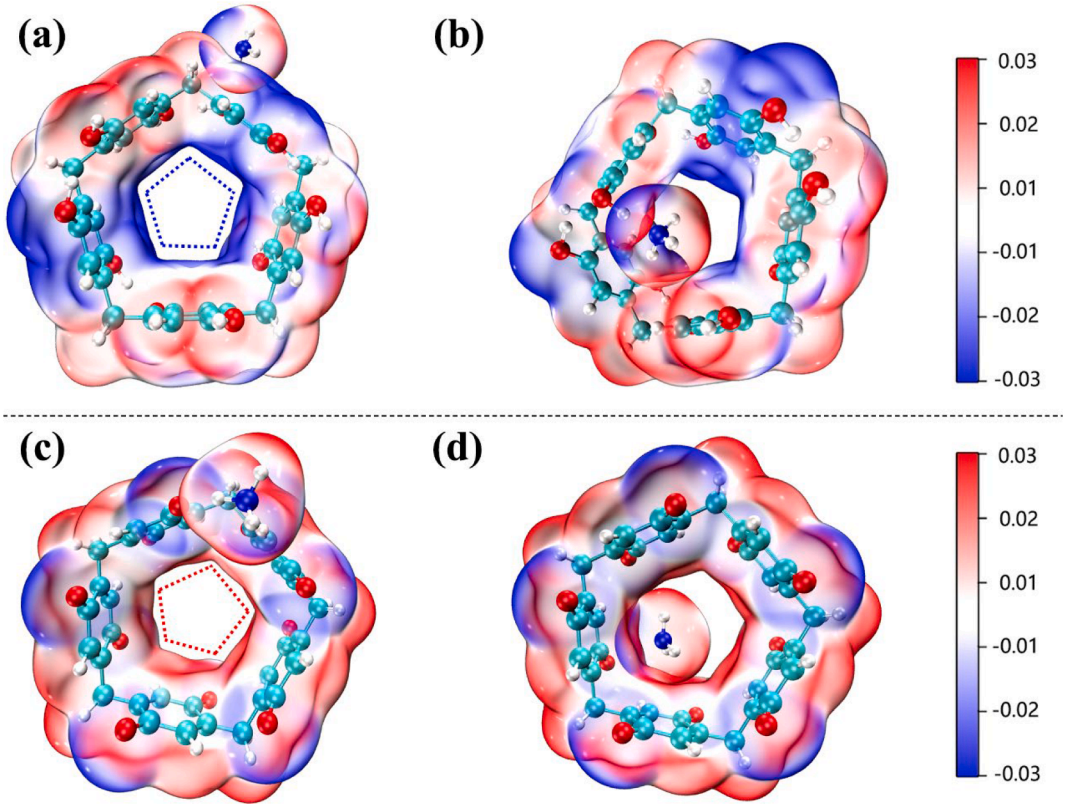

Fig. 8. Molecular ESP values mapped on van der Waals surface of (a) OHP[5], (b) OHP[5]-NH_3 cluster, (c) P[5]Q, and (d) P[5]Q-NH_3 cluster (negative regions are indicated in blue, and the positive regions are indicated in red). (For interpretation of the references to color in this figure legend, the reader is referred to the web version of this article.)

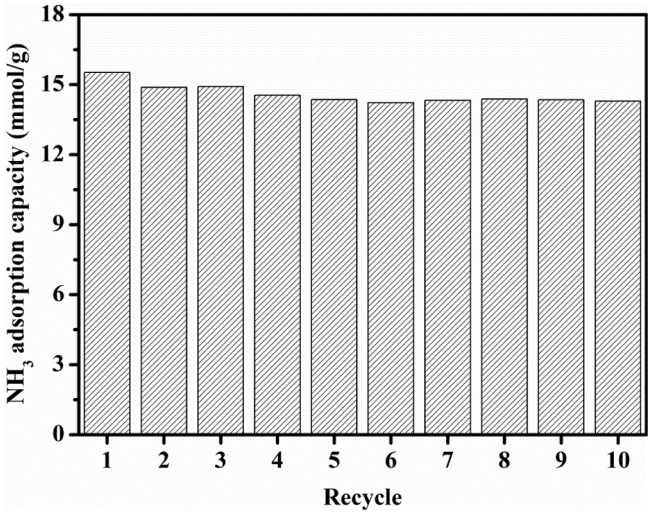

Fig. 9. Reusability of P[5]Q in NH_3 adsorption–desorption cycles.

4. Conclusion

In summary, two kinds of pillar[5]arenes, OHP[5] and P[5]Q, were successfully prepared to perform rapid capture and efficient recovery of NH_3. The unique geometric features and chemical structures of the two pillar[5] arenes exhibited high NH_3 adsorption capacities. P[5]Q obtained from the oxidation of OHP[5] showed superior NH_3 adsorption performance owing to the higher adsorption strength for NH_3 and the electron-deficient internal cavity with a diameter of 0.56 nm. Dynamic breakthrough experiments also show that P[5]Q has good separation performance on low concentration NH_3. Using functional groups to design pillar[5]arenes to adsorb NH_3 provides a new strategy for NH_3 recovery.

CRediT authorship contribution statement

Wen-Qiang Gong: Investigation, Writing – original draft, Data curation. **Yu-Xuan Fu:** Methodology, Investigation. **Yan Zhou:** Methodology, Investigation. **Ming-Shuai Sun:** Methodology, Investigation, Writing – review & editing. **Zhang-Min Li:** Methodology, Writing – review & editing. **Nai-Hao Lu:** Methodology, Resources. **Duan-Jian Tao:** Supervision, Conceptualization, Funding acquisition, Resources, Writing – review & editing.

Declaration of Competing Interest

The authors declare that they have no known competing financial interests or personal relationships that could have appeared to influence the work reported in this paper.

Data availability

Data will be made available on request.

Acknowledgements

We thank the Key Lab of Fluorine and Silicon for Energy Materials and Chemistry of Ministry of Education, Jiangxi Normal University (KFSEMC-202209) for the financial support.

Appendix A. Supplementary material

Supplementary data to this article can be found online at https://doi.org/10.1016/j.seppur.2023.124304.

References

[1] S. Giddey, S.P.S. Badwal, C. Munnings, M. Dolan, Ammonia as a renewable energy transportation media, ACS Sustain. Chem. Eng. 5 (11) (2017) 10231–10239.
[2] J.H. Montoya, C. Tsai, A. Vojvodic, J.K. Nørskov, The challenge of electrochemical ammonia synthesis: A new perspective on the role of nitrogen scaling relations, ChemSusChem 8 (13) (2015) 2180–2186.
[3] J. Guo, P. Chen, Catalyst: NH_3 as an energy carrier, Chem 3 (5) (2017) 709–712.
[4] Y. Kojima, M. Yamaguchi, Ammonia storage materials for nitrogen recycling hydrogen and energy carriers, Int. J. Hydrogen Energy 45 (16) (2020) 10233–10246.
[5] B. Pan, S.K. Lam, A. Mosier, Y. Luo, D. Chen, Ammonia volatilization from synthetic fertilizers and its mitigation strategies: A global synthesis, Agr. Ecosyst. Environ. 232 (2016) 283–289.
[6] H. Jasuja, G.W. Peterson, J.B. Decoste, M.A. Browe, K.S. Walto, Evaluation of MOFs for air purification and air quality control applications: Ammonia removal from air, Chem. Eng. Sci. 124 (2014) 118–124.
[7] D.D. Cao, Z.Y. Li, Z.Z. Wang, H.Y. Wang, S.Q. Gao, Y. Wang, Y.L. Shi, J.K. Qiu, Y. Zhao, J.J. Wang, Highly dispersed ionic liquids in mesoporous molecular sieves enable a record NH_3 absorption, ACS Sustain. Chem. Eng. 9 (2021) 16363–16372.
[8] S. Kang, J. Roh, E.C. Jeon, Estimating the characteristics and emission factor of ammonia from sewage sludge incinerator, Int. J. Env. Res. Pub. He. 18 (5) (2021) 2539.
[9] Y.Y. Guo, B.L. Mu, P.F. Liu, L. Luo, L.W. Hao, Y.M. Li, T.Y. Zhu, Ammonia emission estimation for the cement industry in northern China, Atmos. Pollut. Res. 11 (10) (2020) 1738–1742.
[10] Y. Chen, Q.R. Zhang, X.R. Cai, H.R. Zhang, H.M. Lin, C.Y. Zheng, Z.Q. Guo, S.Y. Hu, L. Chen, S. Tao, M.D. Liu, X.J. Wang, Rapid increase in China's industrial ammonia emissions: evidence from unit-based mapping, Environ. Sci. Tech. 56 (6) (2022) 3375–3385.
[11] S. Kang, Y.J. Hong, S.D. Kim, E.C. Jeon, Ammonia emission factors and uncertainties of coke oven gases in iron and steel industries, Sustainability 12 (9) (2020) 3518.
[12] W. Ouyang, Z.M. Lian, X. Hao, X. Gu, F.H. Hao, C.Y. Lin, F. Zhou, Increased ammonia emissions from synthetic fertilizers and land degradation associated with reduction in arable land area in China, Land Degrad. Dev. 29 (11) (2018) 3928–3939.
[13] J.L. Wang, S.J. Zeng, F. Huo, D.W. Shang, H.Y. He, L. Bai, X.P. Zhang, J.W. Li, Metal chloride anion-based ionic liquids for efficient separation of NH_3, J. Clean. Prod. 206 (2019) 661–669.
[14] S.J. Zeng, L. Liu, D.W. Shang, J.P. Feng, H.F. Dong, Q.X. Xu, X.P. Zhang, S.J. Zhang, Efficient and reversible absorption of ammonia by cobalt ionic liquids through Lewis acid-base and cooperative hydrogen bond interactions, Green Chem. 20 (9) (2018) 2075–2083.
[15] S.J. Zeng, Y.K. Cao, P.F. Li, X.Y. Liu, X.P. Zhang, Ionic liquid-based green processes for ammonia separation and recovery, Curr. Opin. Green Sustain. Chem. 25 (2020) 100354.
[16] X.Q. Sun, G.L. Li, S.J. Zeng, L. Yuan, L. Bai, X.P. Zhang, Ultra-high NH_3 absorption by triazole cation-functionalized ionic liquids through multiple hydrogen bonding, Sep. Purif. Technol. 307 (2023) 122825.
[17] Y. Chen, X.X. Han, Z.H. Liu, D.K. Yu, W.X. Guo, T.C. Mu, Capture of toxic gases by deep eutectic solvents, ACS Sustain. Chem. Eng. 8 (14) (2020) 5410–5430.
[18] G. Cui, M. Lv, D.Z. Yang, Efficient CO_2 absorption by azolide-based deep eutectic solvents, Chem. Commun. 55 (10) (2019) 1426–1429.
[19] T.X. Zhao, J. Liang, Y.T. Zhang, Y.T. Wu, X.B. Hu, Unexpectedly efficient SO_2 capture and conversion to sulfur in novel imidazole-based deep eutectic solvents, Chem. Commun. 54 (65) (2018) 8964–8967.
[20] W. Xu, H. Chen, K. Jie, Z. Yang, T. Li, S. Dai, Entropy-driven mechanochemical synthesis of polymetallic zeolitic imidazolate frameworks for CO_2 fixation, Angew. Chem. Int. Ed. 131 (15) (2019) 5072–5076.
[21] C.J. Doonan, D.J. Tranchemontagne, T.G. Glover, J.R. Hunt, O.M. Yaghi, Exceptional ammonia uptake by a covalent organic framework, Nat. Chem. 2 (3) (2010) 235–238.
[22] H. Wang, X. Zeng, W. Wang, D. Cao, Selective capture of trace sulfur gas by porous covalent-organic materials, Chem. Eng. Sci. 135 (2015) 373–380.
[23] P. Kuhn, M. Antonietti, A. Thomas, Porous, covalent triazine-based frameworks prepared by ionothermal synthesis, Angew. Chem. Int. Ed. 47 (18) (2008) 3450–3453.
[24] Y. Shi, Y. Xie, H. Cui, Y. Ye, H. Wu, W. Zhou, H. Arman, R.B. Lin, B. Chen, Highly selective adsorption of carbon dioxide over acetylene in an ultramicroporous metal-organic framework, Adv. Mater. 33 (45) (2021) 2105880.
[25] J. Liu, Z. Chen, R. Wang, S. Alayoglu, T. Islamoglu, S.-J. Lee, T.R. Sheridan, H. Chen, R.Q. Snurr, O.K. Farha, Zirconium metal-organic frameworks integrating chloride ions for ammonia capture and/or chemical separation, ACS Appl. Mater. Interfaces 13 (19) (2021) 22485–22494.
[26] G. Barin, G.W. Peterson, V. Crocella, J. Xu, K.A. Colwell, A. Nandy, J.A. Reimer, S. Bordiga, J.R. Long, Highly effective ammonia removal in a series of Brønsted acidic porous polymers: Investigation of chemical and structural variations, Chem. Sci. 8 (6) (2017) 4399–4409.
[27] Z.Y. Li, Y. Chen, Z.Z. Wang, Y. Zhao, Q.C. Xia, J.K. Qiu, H.Y. Wang, J.J. Wang, Ionic liquid hybrid metal-organic frameworks for efficient adsorption and selective separation of ammonia at high temperature, Chem. Eng. J. 464 (2023), 142728.
[28] D.W. Kim, D.W. Kang, M. Kang, J.H. Lee, J.H. Choe, Y.S. Chae, D.S. Choi, H. Yun, C.S. Hong, High ammonia uptake of a metal-organic framework adsorbent in a wide pressure range, Angew. Chem. Int. Ed. 59 (50) (2020) 22531–22536.
[29] T. Ogoshi, S. Kanai, S. Fujinami, T.-A. Yamagishi, Y. Nakamoto, Para-bridged symmetrical pillar[5]arenes: Their lewis acid catalyzed synthesis and host-guest property, J. Am. Chem. Soc. 130 (15) (2008) 5022–5023.
[30] Y. Zhou, K. Jie, R. Zhao, E. Li, F. Huang, Highly selective removal of trace isomers by nonporous adaptive pillararene crystals for chlorobutane purification, J. Am. Chem. Soc. 142 (15) (2020) 6957–6961.
[31] Q. Li, K. Jie, F. Huang, Highly selective separation of minimum-boiling azeotrope toluene/pyridine by nonporous adaptive crystals of cucurbit[6]uril, Angew. Chem. 132 (13) (2020) 5393–5396.
[32] T. Ogoshi, R. Sueto, K. Yoshikoshi, T.-A. Yamagishi, One-dimensional channels constructed from per-hydroxylated pillar[6]arene molecules for gas and vapour adsorption, Chem. Commun. 50 (96) (2014) 15209–15211.
[33] E. Li, Y. Zhou, R. Zhao, K. Jie, F. Huang, Dihalobenzene shape sorting by nonporous adaptive crystals of perbromoethylated pillararenes, Angew. Chem. Int. Ed. 58 (12) (2019) 3981–3985.
[34] L. Tan, Y. Zhu, H. Long, Y. Jin, W. Zhang, Y. Yang, Pillar[n]arene-based supramolecular organic frameworks with high hydrocarbon storage and selectivity, Chem. Commun. 53 (48) (2017) 6409–6412.
[35] Y.J. Zhou, K.C. Jie, R. Zhao, E. Li, F.H. Huang, Highly selective removal of trace isomers by nonporous adaptive pillararene crystals for chlorobutane purification, J. Am. Chem. Soc. 142 (2020) 6957–6961.
[36] T. Ogoshi, T. Akoi, K. Kitajima, S. Fujinami, T. Yamagishi, Y. Nakamoto, Facile, rapid, and high-yield synthesis of pillar[5]arene from commercially available reagents and its x-ray crystal structure, J. Org. Chem. 76 (1) (2011) 328–331.
[37] F. Mijangos, F. Varona, N. Villota, Changes in solution color during phenol oxidation by fenton reagent, Environ. Sci. Tech. 40 (17) (2006) 5538–5543.
[38] F.F. Chen, K. Huang, Y. Zhou, Z. Tian, X. Zhu, D.J. Tao, S. Dai, Multi-molar absorption of CO_2 by the activation of carboxylate groups in amino acid ionic liquids, Angew. Chem. Int. Ed. 128 (25) (2016) 7282–7286.
[39] M.J. Frisch, G.W. Trucks, H.B. Schlegel, G.E. Scuseria, M.A. Robb, J.R. Cheeseman, G. Scalmani, V. Barone, G.A. Petersson, H. Nakatsuji, X. Li, M. Caricato, A.V. Marenich, J. Bloino, B.G. Janesko, R. Gomperts, B. Mennucci, H.P. Hratchian, J.V. Ortiz, A.F. Izmaylov, J.L. Sonnenberg, Williams, F. Ding, F. Lipparini, F. Egidi, J. Goings, B. Peng, A. Petrone, T. Henderson, D. Ranasinghe, V.G. Zakrzewski, J. Gao, N. Rega, G. Zheng, W. Liang, M. Hada, M. Ehara, K. Toyota, R. Fukuda, J. Hasegawa, M. Ishida, T. Nakajima, Y. Honda, O. Kitao, H. Nakai, T. Vreven, K. Throssell, J.A. Montgomery Jr., J.E. Peralta, F. Ogliaro, M.J. Bearpark, J.J. Heyd, E.N. Brothers, K.N. Kudin, V.N. Staroverov, T.A. Keith, R. Kobayashi, J. Normand, K. Raghavachari, A.P. Rendell, J.C. Burant, S.S. Iyengar, J. Tomasi, M. Cossi, J.M. Millam, M. Klene, C. Adamo, R. Cammi, J.W. Ochterski, R.L. Martin, K. Morokuma, O. Farkas, J.B. Foresman, D.J. Fox, Gaussian 16 rev. C.01, Wallingford, CT, 2016.
[40] F. Weigend, Accurate coulomb-fitting basis sets for H to Rn, PCCP 8 (9) (2006) 1057–1065.
[41] F. Weigend, R. Ahlrichs, Balanced basis sets of split valence, triple zeta valence and quadruple zeta valence quality for H to Rn: design and assessment of accuracy, PCCP 7 (18) (2005) 3297–3305.
[42] Y. Zhao, D.G. Truhlar, The M06 suite of density functionals for main group thermochemistry, thermochemical kinetics, noncovalent interactions, excited states, and transition elements: two new functionals and systematic testing of four M06-class functionals and 12 other functionals, Theor. Chem. Acc. 120 (1) (2008) 215–241.
[43] T. Lu, F. Chen, Multiwfn: A multifunctional wavefunction analyzer, J. Comput. Chem. 33 (5) (2012) 580–592.
[44] M. Schwanninger, J.C. Rodrigues, H. Pereira, B. Hinterstoisser, Effects of short-time vibratory ball milling on the shape of FT-IR spectra of wood and cellulose, Vib. Spectrosc 36 (1) (2004) 23–40.
[45] B. Hinterstoisser, M. Åkerholm, L. Salmén, Effect of fiber orientation in dynamic ftir study on native cellulose, Carbohydr. Res. 334 (1) (2001) 27–37.
[46] Z. Zhang, H. Li, S. Sun, L. Huang, I. Noda, Differentiation of rhizoma curcumas longae and radix curcumae by a multistep infrared macro-fingerprint method, Anal. Lett. 46 (16) (2013) 2597–2609.
[47] A. Drelinkiewicz, M. Hasik, 2-ethyl-9,10-anthraquinone hydrogenation over pd/polymers: Effect of polymers-Pd(II) chlorocomplexes interactions, J. Mol. Catal. A Chem. 177 (1) (2001) 149–164.
[48] A. Popov, E. Kondratieva, J.-P. Gilson, L. Mariey, A. Travert, F. Maugé, IR study of the interaction of phenol with oxides and sulfided CoMo catalysts for bio-fuel hydrodeoxygenation, Catal. Today 172 (1) (2011) 132–135.
[49] I.K. Lee, B.S. Yun, S.M. Cho, W.G. Kim, J.P. Kim, I.J. Ryoo, H. Koshino, I.D. Yoo, Betulinans A and B, two benzoquinone compounds from lenzites betulina, J. Nat. Prod. 59 (11) (1996) 1090–1092.
[50] Q. Tian, L. Jing, S. Ye, J. Liu, R. Chen, C.-A.-H. Price, F. Fan, J. Liu, Nanospatial charge modulation of monodispersed polymeric microsphere photocatalysts for exceptional hydrogen peroxide production, Small 17 (49) (2021) 2103224.
[51] L. Xu, J. Zhang, J. Ding, T. Liu, G. Shi, X. Li, W. Dang, Y. Cheng, R. Guo, Pore structure and fractal characteristics of different shale lithofacies in the dalong formation in the western area of the lower yangtze platform, Minerals 10 (1) (2020) 72.
[52] L. Zhao, F. Luo, M. Zhai, H. Mitomo, F. Yoshii, Study on CM-chitosan/activated carbon hybrid gel films formed with EB irradiation, Radiat. Phys. Chem. 77 (5) (2008) 622–629.

[53] D.A. Reddy, E.H. Kim, M. Gopannagari, R. Ma, P. Bhavani, D.P. Kumar, T.K. Kim, Enhanced photocatalytic hydrogen evolution by integrating dual co-catalysts on heterophase CdS nano-junctions, ACS Sustain. Chem. Eng. 6 (10) (2018) 12835–12844.
[54] X. Zhu, C. Tian, G.M. Veith, C.W. Abney, J.r.m. Dehaudt, S. Dai, In situ doping strategy for the preparation of conjugated triazine frameworks displaying efficient CO_2 capture performance, J. Am. Chem. Soc. 138 (36) (2016) 11497–11500.
[55] C. Marsh, X. Han, J. Li, Z. Lu, S.P. Argent, I.D. Silva, Y. Cheng, L.L. Daemen, A. J. Ramirez-Cuesta, S.P. Thompson, A.J. Blake, S. Yang, M. Schroder, Exceptional packing density of ammonia in a dual-functionalized metal-organic framework, J. Am. Chem. Soc. 143 (17) (2021) 6586–6592.
[56] A.J. Rieth, Y. Tulchinsky, M. Dinca, High and reversible ammonia uptake in mesoporous azolate metal-organic frameworks with open Mn Co, and Ni sites, J. Am. Chem. Soc. 138 (30) (2016) 9401–9404.